Calcium-Induced Conformational Switching of *Paramecium* Calmodulin Provides Evidence for Domain Coupling†

Olav R. Jaren,‡,§ James K. Kranz,‡,|| Brenda R. Sorensen,§ A. Joshua Wand,|| and Madeline A. Shea*,§

Department of Biochemistry, Roy J. and Lucille A. Carver College of Medicine, University of Iowa, Iowa City, Iowa 52242-1109, and Department of Biochemistry and Biophysics, University of Pennsylvania School of Medicine, Philadelphia, Pennsylvania 19104-6059

Received June 21, 2002; Revised Manuscript Received September 24, 2002

ABSTRACT: Calmodulin (CaM) is an intracellular calcium-binding protein essential for many pathways in eukaryotic signal transduction. Although a structure of Ca^{2+}-saturated *Paramecium* CaM at 1.0 Å resolution (1EXR.pdb) provides the highest level of detail about side-chain orientations in CaM, information about an end state alone cannot explain driving forces for the transitions that occur during Ca^{2+}-induced conformational switching and why the two domains of CaM are saturated sequentially rather than simultaneously. Recent studies focus attention on the contributions of interdomain linker residues. Electron paramagnetic resonance showed that Ca^{2+}-induced structural stabilization of residues 76−81 modulates domain coupling [Qin and Squier (2001) *Biophys. J. 81*, 2908−2918]. Studies of N-domain fragments of *Paramecium* CaM showed that residues 76−80 increased thermostability of the N-domain but lowered the Ca^{2+} affinity of sites I and II [Sorensen et al. (2002) *Biochemistry 41,* 15−20]. To probe domain coupling during Ca^{2+} binding, we have used $^{1}H-^{15}N$ HSQC NMR to monitor more than 40 residues in *Paramecium* CaM. The titrations demonstrated that residues Glu78 to Glu84 (in the linker and cap of helix E) underwent sequential phases of conformational change. Initially, they changed in volume (slow exchange) as sites III and IV titrated, and subsequently, they changed in frequency (fast exchange) as sites I and II titrated. These studies provide evidence for Ca^{2+}-dependent communication between the domains, demonstrating that spatially distant residues respond to Ca^{2+} binding at sites I and II in the N-domain of CaM.

Calmodulin (CaM)[1] is a small (148 residue) eukaryotic Ca^{2+}-binding protein that is required for regulation of a diverse range of target enzymes in a Ca^{2+}-dependent manner. The protein has two primary structural domains; each contains a pair of helix−loop−helix Ca^{2+}-binding motifs, termed EF-hand motifs (Figure 1) (cf. ref *1*). Sites III and IV of the C-terminal domain have micromolar affinity for Ca^{2+}, while sites I and II in the N-terminal domain have a reduced affinity (*2*, *3*); ligation of Ca^{2+} to either pair of sites is highly cooperative (*4*, *5*). The residues that chelate Ca^{2+} within each globular domain are highly conserved among all four sites (Figure 1B) and among CaM from different organisms. Structures of both apo and Ca^{2+}-saturated states of CaM indicate structural transitions occur within each domain in response to Ca^{2+} binding. Solution studies indicate that the two globular domains are bridged by a linker that is dynamically disordered in both the apo and Ca^{2+}-saturated states of the protein (*6*−*8*).

Despite evidence that this linker is dynamically disordered and that the two globular domains are structurally independent, there is strong evidence of interdomain communication that affects CaM function. Studies of an isolated N-terminal domain (residues 1−75) fragment and the complementary C-terminal domain (residues 76−148) fragment indicate that affinity of Ca^{2+} for the isolated N-terminal domain is reduced in the context of the full protein relative to Ca^{2+} affinity in the isolated domain (*2*). The results are consistent with the presence of negative cooperativity between domains, where the physical connection of the N-terminal domain to the C-terminal domain through the dynamic linker gives rise to a reduced affinity of Ca^{2+} to sites I and II of the N-terminal domain. However, the sources of domain-specific differences in Ca^{2+} affinity are still poorly understood in detail.

Studying residue-specific behavior during the transition from the apo to the fully saturated states may offer insight into this issue. The interactions between helices that flank EF-hands are of particular relevance to observed differences in Ca^{2+}-binding affinity for pairs of sites in either the N- or C-terminal domains. Early proton NMR studies of the calcium-induced changes in mammalian CaM monitored approximately 10 residues (*9*, *10*) and were identified by reference to assignments in its tryptic fragments (*11*). Although a few of these residues were initially reported to

† These studies were supported by an American Heart Association predoctoral fellowship to O.R.J., an NRSA postdoctoral fellowship to J.K.K. (F32 GM20206-01), an NIH award to A.J.W. (DK39806), and an NIH award to M.A.S. (R01 GM 57001).

* Corresponding author. Telephone: (319) 335-7885. Fax: (319) 335-9570. E-mail: madeline-shea@uiowa.edu.

‡ These authors contributed equally to this work.

§ University of Iowa.

|| University of Pennsylvania School of Medicine.

[1] Abbreviations: CaM, calmodulin; DSS, 2,2-dimethyl-2-silapentane-5-sulfonatel EPR, electron paramagnetic resonance; FRET, fluorescence resonance energy transfer; HSQC, heteronuclear single-quantum coherence; PCaM, *Paramecium* calmodulin; RCaM, rat calmodulin.

10.1021/bi026340+ CCC: $22.00
Published on Web 11/06/2002

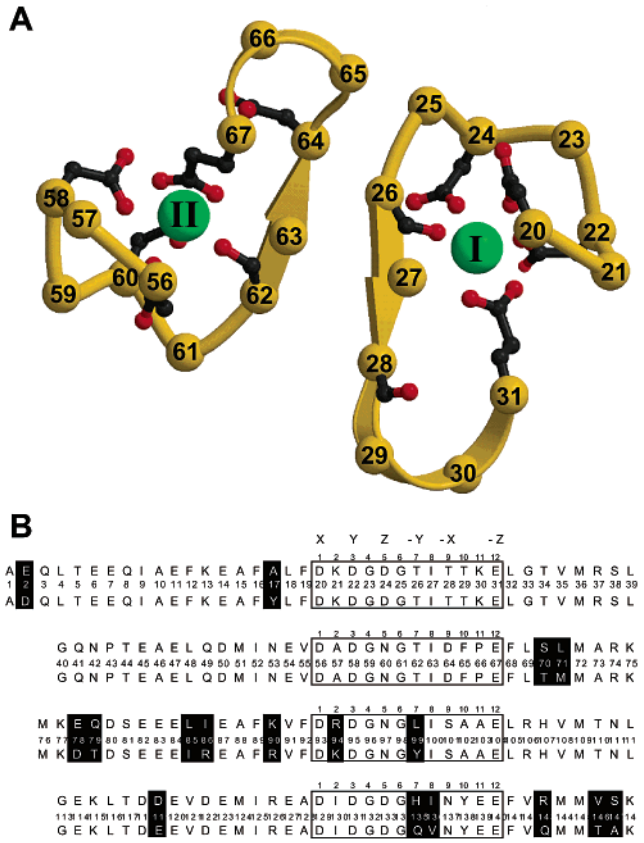

FIGURE 1: (A) Diagram of Ca^{2+}-binding sites I and II of PCaM. Ca^{2+} ions are shown as green spheres. Residues that ligate Ca^{2+} are depicted in the ball-and-stick format. α carbons for all residues in each site are shown as gold spheres labeled by residue number. This depiction was based on crystal structure coordinates of 1clm.pdb (*62*) using the programs Molscript (*69*) and Raster3D (*70*). (B) Amino acid sequences of PCaM (top) and RCaM (bottom) aligned by sequences of the Ca^{2+}-binding sites (in boxes). Sequence differences are indicated by shaded residues. The letters above site I indicate positions of Ca^{2+} chelation groups. The numbers above each site refer to the position in the binding site sequence.

respond to calcium binding to both domains (*9*, *10*), this was later revised upon refinement of resonance assignments (*12*, *13*). Chemical modification and quantitative proteolytic footprinting of calcium titrations of CaM provided evidence for at least one populated ligation intermediate whose structural properties are distinct from both of the end states (*2*, *14*−*21*). Analysis of site knockout mutants of CaM (*19*, *22*−*24*) and yeast CaM (*13*) indicated that sequence changes in the C-terminal domain that lowered calcium affinity of sites III or IV increased the calcium affinity of sites I and II, demonstrating that structural and energetic effects were propogated from one domain to the other. However, there are no reports of interdomain NOEs in calmodulin at any level of calcium saturation. Therefore, it is unlikely that any persistent short-range contacts underlie the energetics of interdomain interactions.

Although an NMR-based structural analysis of Ca^{2+}-saturated CaM found the interdomain residues to be dynamically disordered (*25*−*27*), we now know that these residues contribute to the energetic properties of CaM. For example, deletion of residues M76−D80 from an N-domain fragment of CaM decreased the stability of the apo domain by ~9 °C and increased its Ca^{2+} affinity by a factor of 4 (*28*) and illustrated long-range effects of the interdomain linker on the energetics of this domain fragment. Spectroscopic studies by Squier and co-workers have also demonstrated that the interdomain linker residues provide a Ca^{2+}-regulated conformational switch that couples the N- and C-domains (*29*−*32*).

To probe the relationship between the Ca^{2+}-dependent behavior of residues at the interdomain boundary and their contribution to regulation of CaM function, we have used $^{1}H-^{15}N$ HSQC NMR to monitor conformational changes in the protein backbone of *Paramecium* CaM (PCaM) as a function of increasing calcium. We monitored the changes in intensity and chemical shift of 40 residues in PCaM: 17 residues between A1 and K75 in the N-domain, 5 in the span of R76 to E84, and 18 in the span from L85 to K148 in the C-domain. As expected, the greatest Ca^{2+}-induced conformational changes were observed for residues within the four Ca^{2+}-binding sites. Resonances for most residues in the N-domain did not change in chemical shift between zero and two Ca^{2+} equivalents. However, many were found to be in intermediate exchange over the entire course of the titration, and the intensity of several resonances dropped below detectable limits.

Unique to this study is our observation that residues 78−84 in PCaM (in the interdomain linker and cap of helix E) switched allegiance over the course of a stoichiometric titration. Between zero and two Ca^{2+} equivalents, they behaved like many residues in the C-domain. NMR cross-peaks for these residues were in slow exchange on the NMR chemical shift time scale, with two separate resonances corresponding to apo and Ca^{2+}-saturated states; intensities of these peaks titrated along with the titration of Ca^{2+}-binding sites III and IV over the addition of the first 2 molar equiv of calcium. However, between two and four Ca^{2+} equivalents, those residues changed their response to added Ca^{2+} and behaved like the majority of residues in the N-domain as sites I and II became fully saturated with calcium, consistent with the changes observed for most residues located in sites I and II. These results suggest the presence of structural coupling between the N- and C-domains of CaM through residues at the interdomain boundary.

MATERIALS AND METHODS

Protein Purification. Reagent chemicals were of the highest grade commercially available. The PCaM gene was overexpressed in JM109 cells (gifts from C. Kung, University Wisconsin—Madison). The rat CaM (RCaM) gene was overexpressed in BL21(DE3) pLysS cells (*20*). Bacterial cells were grown in minimal media containing 1 g/L [^{15}N]-ammonium chloride with or without 10 g/L [^{13}C]glucose (Cambridge Isotopes, Andover, MA). Calmodulin was purified as described (*33*) with modifications. Following hydrophobic interaction chromatography, CaM-containing fractions were heated at 80 °C for 10 min in 10 mM $CaCl_2$, 20 mM Tris, and 3 mM DTT, pH 7.4. The precipitate was separated from the soluble protein by centrifugation at 5K rpm and filtration through a 0.22 μm filter (Millipore). The filtered solution was dialyzed into 50 mM HEPES and 100 mM KCl and purified further on a HiLoad 26/60 Superdex 75 column by FPLC (Pharmacia). Purity of the proteins was assessed by reversed-phase HPLC and silver nitrate staining of SDS−PAGE gels. The protein was judged to be 99% pure.

NMR Sample Preparation. RCaM and PCaM were dialyzed against 5 mM EGTA and 20 mM HEPES, pH 7.3, to remove excess Ca^{2+} and subsequently dialyzed against 50 mM HEPES, 100 mM KCl, and 50 μM EGTA, pH 7.40. Concentrated proteins were diluted into the same buffer, except that it contained 10% D_2O and 5 μM DSS (for the Cd^{2+} titration, the sample contained 20% D_2O and no DSS). The starting protein concentration for both Ca^{2+} and Cd^{2+} titrations was 1.3 mM as determined by amino acid analysis (Molecular Analysis Facility, University of Iowa). CaM samples used for NMR assignment experiments were equilibrated using gel permeation chromatography. Apo conditions were 1.0 mM PCaM, 10 mM imidazole-d_4, 25 mM KCl, 50 μM EGTA, 0.01% NaN_3, pH 6.5, and 8% D_2O. Ca^{2+}-saturated conditions were 1.25 mM PCaM, 10 mM imidazole-d_4, 100 mM KCl, 5 mM $CaCl_2$, 0.01% NaN_3, pH 6.5, and 8% D_2O. Protein integrity was tested by HPLC, SDS−PAGE, and MS analysis of aliquots over a multiweek period.

NMR Assignments of Apo and Ca^{2+}-Saturated PCaM. NMR spectra were recorded on Varian INOVA spectrometers at 500, 600, and 750 MHz (^{1}H) (University of Pennsylvania). Each spectrometer was equipped with a standard Varian 5 mm triple resonance probe with triple-axis pulsed-field gradients. Proton chemical shifts were referenced to an external standard of DSS in D_2O; ^{13}C and ^{15}N chemical shifts were determined from the ^{1}H (*34*). The sample temperature was 298 K for Ca^{2+}-saturated PCaM and 302 K for apo PCaM.

The assignments of H^N, N, C^α, C^β, and C′ atoms of ^{13}C,^{15}N-labeled PCaM were determined using the following pulsed-field gradient NMR pulse sequences: (1) ^{1}H−^{15}N HSQC (*35*); (2) ^{1}H−^{13}C constant time HSQC (*36*); (3) CBCA(CO)NH (*37*, *38*); (4) HNCACB (*38*, *39*); (5) HNCO (*38*, *40*); (6) HN(CA)CO (*41*); (7) CTSL-HCANH (*42*); and (8) ^{15}N-edited 3D NOESY(*35*). All 3D experiments were recorded with a spectral width of 12.8 ppm in the proton dimension with the carrier frequency set at the center of the H_2O resonance and a spectral width of 34.5 ppm in the nitrogen dimension (carrier set to 119 ppm). ^{13}C spectral widths were 53 ppm in CBCA(CO)NH and HNCACB experiments (carrier set to 43 ppm), 33 ppm in the CTSL-HCANH experiment (carrier set to 58 ppm), and 12 ppm in HNCO and HN(CA)CO experiments (carrier set to 176 ppm). The 3D NOESY data were recorded using a 70 ms mixing time. Quadrature detection in the indirect time domain was accomplished using the method of States and co-workers (*43*). ^{15}N-resolved experiments employed *z*-axis pulsed-field gradient sensitivity enhancement (*44*−*46*). Solvent suppression was achieved in all experiments with both H_2O flip-back pulses and pulsed-field gradients (*35*, *47*). No irradiation was applied for samples dissolved in D_2O. All spectra were processed using the software package FELIX (Molecular Simulations Inc.). Processed spectra were examined with NMRView (Bruce Johnson, Merck, Rahway, NJ). Assignments were manually determined by identifying linked spin systems and determining their amino acid content from the C^α/C^β chemical shifts (*47*, *48*). The backbone atom assignments were 99% complete. Under apo conditions, the chemical shifts of all of the atoms of A1 and E2, the C^α and C^β atoms of R126, and the C^α atom of G134 were not assigned. Under Ca^{2+}-saturating conditions, the resonances of residues A1 and E2 and the C′ shifts of E7, A10, T28, N42, L48, M51, G59, F65, P66, M72, M76, F92, A102, R106, H107, N111, E120, V121, E123, M124, A128, Y138, F141, R143, M144, and K148 were not assigned. Complete lists of the resonance assignments are given as Supporting Information. No interdomain amide−amide NOEs were observed.

Calcium Titrations Monitored by NMR. Calcium titrations were monitored by sensitivity-enhanced ^{15}N−^{1}H HSQC NMR at 22 °C (*45*) using an INOVA 500 with *z*-axis pulsed-field gradients (College of Medicine NMR Facility, University of Iowa). Each HSQC had 1024 points, 256 increments, and 8 transients per increment with a 2 s recycle delay. The spectral widths were 14 ppm for ^{1}H and 49 ppm for ^{15}N. The delay between scans was 2 s. The total scan time was 2.5 h. The spectra were processed with VNMR 6.1B software (Varian) and zero-filled 1024 points in the ^{1}H dimension and 512 points in the ^{15}N dimension. For Figures 5 and 7, the HSQC and ^{1}H cross section spectra were processed with FELIX. Chemical shifts were referenced to an external DSS standard. The spectra were processed identically.

The titrant solution was 61.7 mM $CaCl_2$ (determined by atomic absorbance with precision of 2%) in a buffer otherwise matching that of the dialyzed protein. The total volume added was 60 μL. The pH changed by less than 0.02 unit during the titration. Chemical shifts and peak intensities were determined from the processed spectra using FELIX; changes were normalized for comparison.

The sensitivity of amide resonances in the ^{1}H−^{15}N HSQC spectrum to Ca^{2+} binding was compared using a weighted average of chemical frequency changes (Figure 1C, Supporting Information). This was expressed as the square root of the sum of the squares of chemical frequency differences in the ^{1}H and ^{15}N dimensions between the apo and Ca^{2+}-saturated positions for each residue as given in eq 1.

$$\Delta f = [(\Delta\delta_{^1H}(500.28\ \text{Hz/ppm}))^2 + (\Delta\delta_{^{15}N}(50.7\ \text{Hz/ppm}))^2]^{1/2} \quad (1)$$

Calcium dissociation rates (Supporting Information) were estimated from the chemical shift differences (in frequency) of the end states relative to the type of resonance exchange behavior observed during the titration. The frequency differences of the ^{15}N and ^{1}H dimensions were considered separately in these measurements, and the greater of these was considered to make the primary contribution to line broadening.

Cadmium Titrations Monitored by NMR. Cadmium-113 NMR spectra were acquired on a 9.4 T Bruker instrument at 88.7 MHz and 25 °C (High-Field NMR Facility, University of Iowa). Chemical shifts were referenced to external (natural abundance isotope) 0.1 M $Cd(ClO_4)_2$. A stock solution of $^{113}CdCl_2$ was prepared from ^{113}CdO (Oakridge; gift from R. Cohen, University of Iowa) by dissolving it in HCl and adjusting the pH to 6.0. Its concentration was measured by atomic absorbance. The NMR acquisition time was 0.4 s/scan, the delay between scans was 1.6 s, and the pulse width was 7.7 μs, corresponding to a 30° tip angle. Each spectrum in the titration was generated from 23400 scans (13 h acquisition). The spectral width was 450 ppm.

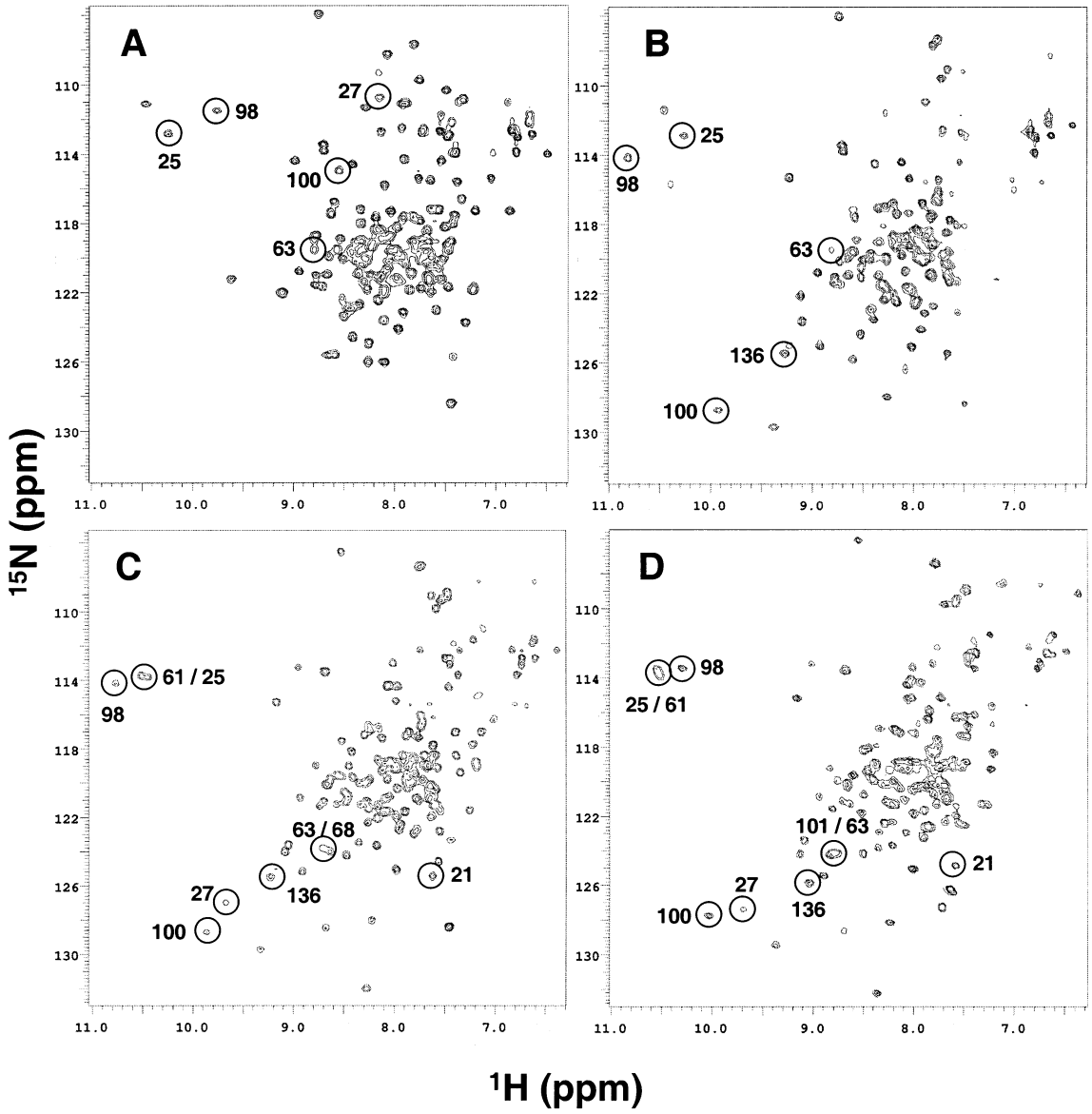

FIGURE 2: $^{1}H-^{15}N$ HSQC spectra of (A) apo PCaM, (B) PCaM at a Ca^{2+}/CaM ratio of 1.93, (C) Ca^{2+}-saturated PCaM, and (D) Ca^{2+}-saturated RCaM. Circled resonances represent a subset of assigned resonances that are used for comparison of chemical shift differences.

The total volume of added Cd^{2+} solution was 100 μL, causing a net decrease in pH of 0.1 unit. Intensities of Cd^{2+} peaks were measured directly from the spectra at −85 and −114 ppm using XWINNMR software (Bruker Analytische Messtechnik GmbH) and were normalized for changes in the protein concentration. The spectra were similar to the spectra of Cd^{2+}-saturated CaM (*49*, *50*).

Secondary Structure. Secondary structure was predicted from a consensus indicated by three different types of information (see Figure 2 in Supporting Information). N-Terminal helix-capping motifs (N-CAP) were predicted using the method described by Gronenborn and Clore (*51*). Helices were also predicted by the pattern of amide−amide NOEs. A helical region was assigned to any sequence of residues with (i, i + 1) NOEs, including gaps up to one residue in length. The CSI program was used to predict secondary structure based on N, C^{α}, C^{β}, and C′ chemical shifts (*52*; http://www.pence.ca). The CSI measurements were used to identify β-strand regions, to support the presence of helices indicated by the NOEs, and to identify the C-termini of the helices.

RESULTS

PCaM HSQC NMR Spectra. More than 60 of 144 $^{1}H-^{15}N$ cross-peaks are sufficiently resolved in the ^{15}N HSQC spectrum of PCaM to be followed throughout the Ca^{2+} titration. Representative spectra for the apo state, partially saturated intermediate state, and Ca^{2+}-saturated state are shown in panels A, B, and C of Figure 2. Most C-domain resonances shifted upon binding the first 2 equiv of Ca^{2+} (e.g., G98 and I100 in Figure 2A,B) while higher Ca^{2+} stoichiometries were required to cause a change in N-domain resonances (e.g., G25 and I63 in Figure 2A−C). A spectrum of Ca^{2+}-saturated vertebrate CaM is provided for comparison in Figure 2D.

Titrations of Sites III and IV. In the C-terminal domain, 30 $^{1}H-^{15}N$ cross-peaks were sufficiently well resolved to be followed throughout the course of the titration. For each residue, complementary changes in peak intensity were observed between two cross-peaks, one corresponding to the apo state and the other to the Ca^{2+}-saturated form. For 12 of the residues, the positions of the apo and Ca^{2+}-saturated

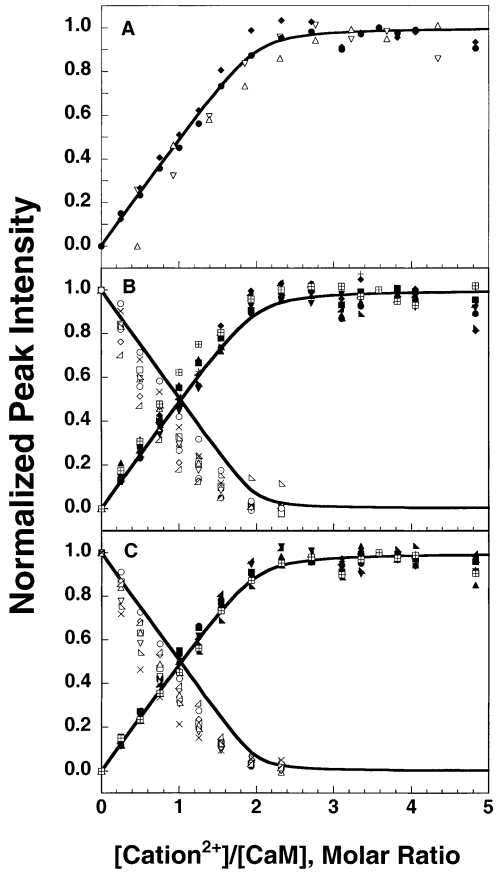

FIGURE 3: Cation titration of sites III and IV of PCaM monitored by changes in peak intensities. (A) Comparative Ca^{2+} titrations of I100 (◆) and I136 (●) with cadmium-113 titrations at −85 ppm (▽) and −114 ppm (△). (B) Normalized changes in peak intensities of resonances at the apo (open symbols) and Ca^{2+} positions (filled symbols) for residues in and surrounding site III: V91 (○●), F92 (□■), R94 (◇◆), N97 (△▲), G98 (▽▼), L99 (triangle open left, triangle solid left), I100 (triangle open right, triangle solid right), A102 (×+), T110 (⊙⊞). (C) Normalized changes in peak intensities of resonances at the apo (open symbols) and Ca^{2+} positions (filled symbols) for residues in and surrounding site IV: G113 (○●), L116 (□■), T117 (◇◆), E127 (△▲), I130 (▽▼), G132 (triangle open left, triangle solid left), I136 (⊞), N137 (triangle open right, triangle solid right), F141 (×+). Simulated trendlines are included to guide the eye.

were such that Δf (eq 1) was less than 0.05 ppm. Overlap made it difficult to determine the intensity of these cross-peaks accurately, and these were not followed beyond 2 molar equiv of calcium. Of the remaining 18 resonances, 9 corresponded to residues in or near site III and 9 were residues in or near site IV.

Figure 3A illustrates that the increases in peak intensities of amide resonances for I100 (position 8 in site III) and I136 (position 8 in site IV) in Ca^{2+}-saturated PCaM were identical to the increases in peak intensity of ^{113}Cd in a Cd^{2+} titration of sites III and IV. The parallel change in peak intensities for the 16 other well-isolated C-domain resonances matched those of I100 and I136, indicating that each of these resonances reported exclusively on binding to site III (Figure 3B) or IV (Figure 3C) within the C-domain.

For all of these, the transition in peak intensity was complete after the addition of the first two Ca^{2+} equivalents. For these resonances reporting on occupancy of sites III and IV, there was no evidence of a chemical shift change resulting from additional exogenous Ca^{2+}, consistent with

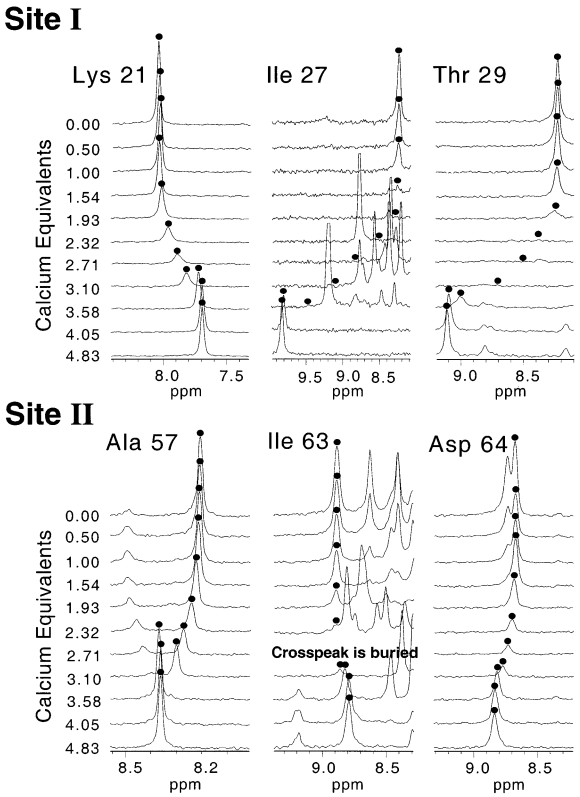

FIGURE 4: Line broadening behavior of N-domain resonances as demonstrated by ^1H cross sections of $^1H-^{15}N$ HSQC spectra. ^1H cross sections are shown for selected Ca^{2+} levels for residues K21, I27, T29 (in site I) and A57, I63, D64 (in site II). A black circle is shown above the resonance that is monitored for each residue. The data for I63 at 2.71 Ca^{2+}/CaM is not shown because the resonance cannot be identified.

slow exchange behavior and high Ca^{2+} affinity of these sites and a lack of responsiveness of C-terminal residues to the ligation state of the N-terminal domain.

Titration of Sites I and II. In the N-domain, 37 resonances were well resolved; for 17 of them, Δf (eq 1) was greater than or equal to 0.05 ppm. Figure 4 shows ^1H cross sections of $^1H-^{15}N$ HSQC spectra for six representative residues in the N-domain: K21, I27, and T29 in site I and A57, I63, and D64 in site II. All of these resonances exhibited changes in both chemical shift and peak intensity upon addition of calcium. Figure 5 compares the Ca^{2+}-dependent change in frequency (top panels) and peak intensity (bottom panels) of 10 residues in or near site I and 7 residues in site II. The chemical shift changes observed for these residues were concerted. Upon addition of the first two Ca^{2+} equivalents, a change of less than 10% was observed. The addition of the second two Ca^{2+} equivalents accounted for almost all of the change, reflecting the response of N-terminal domain amide resonances to the ligation state of sites I and II.

Decreases in peak intensity were observed at lower calcium stoichiometries than were chemical shift changes, with concurrent line broadening of these resonances despite virtually no change in chemical shift in this range of calcium concentrations. The most exaggerated differences were observed for I27 and T29 in site I (Figure 5C) and N60 in site II (Figure 5D), which broadened beyond detection near 1.9 Ca^{2+} equivalents (see ^1H cross sections of the HSQC spectra for I27 and T29 in Figure 4). The total

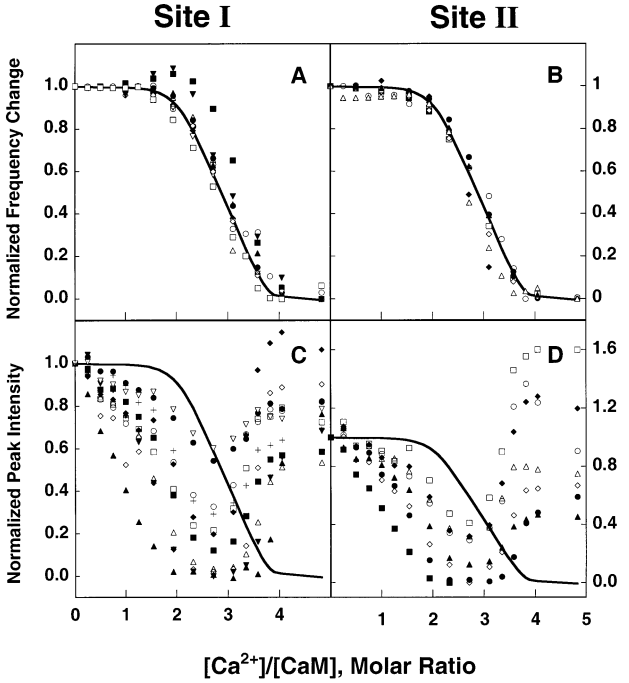

FIGURE 5: Ca^{2+} titration of sites I (left panels) and II (right panels) monitored by changes in frequency (top panels) and $^1H-^{15}N$ HSQC resonance intensity (bottom panels). (A) Normalized change in chemical shift for residues in and surrounding site I: L4 (●), K13 (○), K21 (■), G23 (□), G25 (◆), T26 (◇), I27 (▲), T28 (△), T29 (▼), and G33 (▽). (B) Normalized change in chemical shift for residues in site II: A57 (●), D58 (○), N60 (■), G61 (□), T62 (◆), I63 (◇), D64 (▲), and F65 (△). Simulated trend lines are shown to guide the eye. Changes in peak intensity of residues in these sites were followed by the change in chemical frequency (hertz) as calculated by eq 1. (C) Normalized resonance intensity changes of residues in and surrounding site I: L4 (●) (67 Hz), K13 (○) (104), K21 (■) (188), G23 (□) (193), G25 (◆) (177), T26 (◇) (245), I27 (▲) (725), T28 (△) (268), T29 (▼) (340), G33 (▽) (152), and V35 (+) (215). (D) Normalized resonance intensity changes of residues in site II: A57 (●) (358), D58 (○) (176), N60 (■) (780), G61 (□) (155), T62 (◆) (91), I63 (◇) (231), D64 (▲) (194), and F65 (△) (94). Simulated trend lines illustrate the chemical shift changes for residues in and surrounding sites I and II shown in panels A and B.

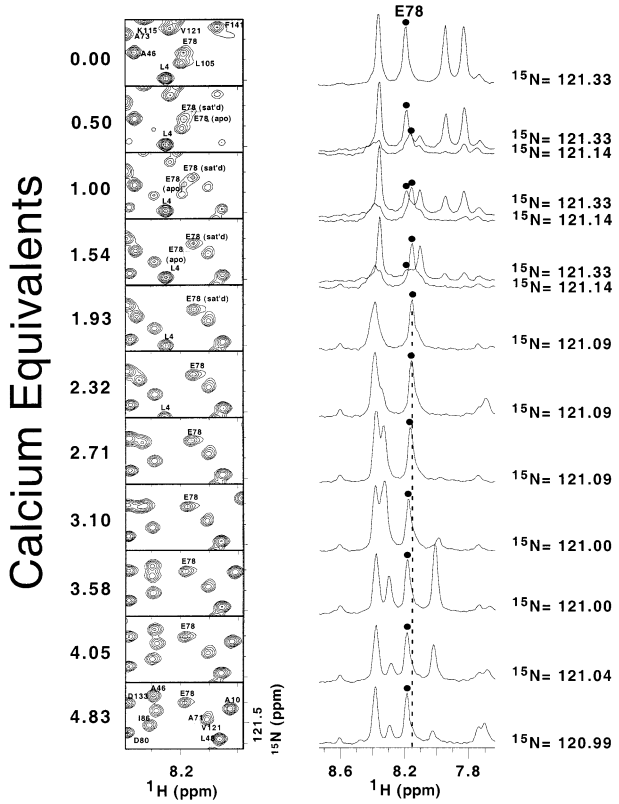

FIGURE 6: Ca^{2+}-dependent behavior of the E78 resonance as monitored by $^1H-^{15}N$ HSQC NMR. Regions of the HSQC spectrum that include the E78 resonance are shown on the left. ^1H cross sections of the HSQC spectra are shown on the right. When two E78 resonances are present in the HSQC spectrum, cross sections for the resonances representing both the apo and Ca^{2+}-saturated conformations are shown and labeled by ^{15}N chemical shift. Dots above the resonances corresponding to E78 are shown to guide the eye. A dotted line corresponding to the chemical shift of the E78 resonance at 1.93 Ca^{2+} equivalents is shown for the ^1H cross sections recorded at the higher Ca^{2+} levels.

chemical shift differences observed for the resonances for I27 (725 Hz) and N60 (780 Hz) were greater than all other positions (which spanned a range of 67−358 Hz; see the legend to Figure 5).

Changes at the Domain Boundaries. Residues in the range of 76− 84 underwent a Ca^{2+}-induced switch in chemical exchange behavior from slow to fast exchange on the NMR chemical shift time scale. Figure 6 illustrates this phenomenon for Glu78, a residue at the border of the N-domain with the interdomain linker. For a subset of 11 Ca^{2+} levels, the pertinent region of the HSQC spectrum and corresponding ^1H cross section are shown. A representation of the normalized changes in frequency and peak intensity for this resonance is shown in Figure 7. With the addition of the first two Ca^{2+} equivalents, both resonances for E78 changed in peak intensity only and were therefore in slow exchange like other C-domain resonances (compare Figures 3 and 7B). However, the addition of the second two Ca^{2+} equivalents resulted in a progressive change in chemical shift. Although the total change was small, it exactly matched the response of residues in or near sites I and II to increasing addition of Ca^{2+} (compare Figure 5A,B and Figure 7A). This behavior was also observed for residues D80, S81, E82, E83, and E84 in the interdomain linker and N-terminal cap of helix E in the C-domain (see Figures 7 and 8).

DISCUSSION

Methods for monitoring Ca^{2+} binding to CaM differ in their ability to measure the occupancy of an individual site, the average properties of a domain (i.e., a pair of sites), or the average occupancy of all four sites (*3*, *4*, *20*, *53*−*55*). Heteronuclear NMR has the unique ability to monitor Ca^{2+}-induced structural changes throughout the backbone, reporting on ligand binding and propagated conformational change. This study of a titration of *Paramecium* CaM focused on determining how residues at the boundary between the two homologous domains behaved relative to those that directly reflect occupancy of the four Ca^{2+}-binding sites.

On the basis of comparisons of structures of apo and Ca^{2+}-saturated CaM from different species available in the literature, it was expected that the greatest changes in secondary structure upon Ca^{2+} binding would occur within the Ca^{2+}-binding sites (*9*, *12*, *56*, *57*). Termini and connecting regions between each of the EF-hand segments in a pair showed little change in chemical shift between the apo and Ca^{2+}-saturated states (illustrated as green spheres in Figure 8). These regions are predicted to have a high propensity

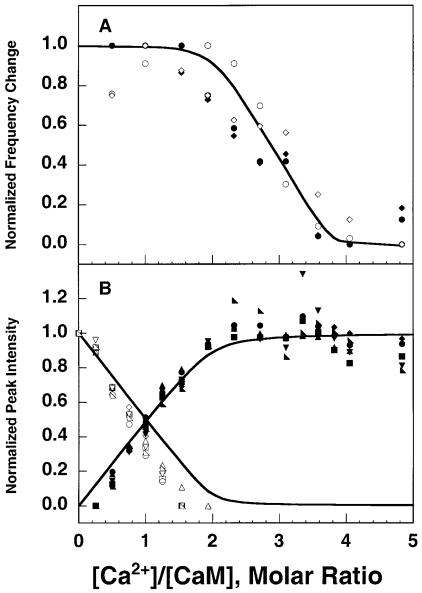

FIGURE 7: Ca^{2+}-dependent behavior of interdomain linker residues monitored by $^{1}H-^{15}N$ HSQC NMR. (A) Normalized changes in ^{1}H chemical shift of resonances E78 (○), S81 (●), E82 (◆), and E84 (◇). (B) Normalized changes in peak intensities of resonances at the apo (open symbols) and Ca^{2+} positions (filled symbols) of E78 (○●), D80 (□■), S81 (◇◆), E82 (△▲), E83 (▽▼), and E84 (triangle open left, triangle solid left). Simulated trend lines are shown to guide the eye.

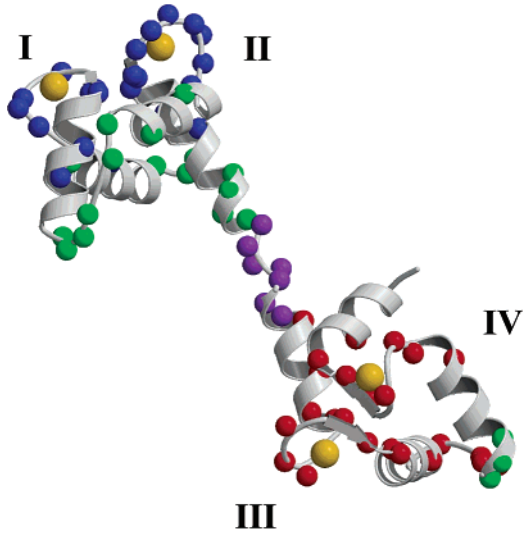

FIGURE 8: Response of amide resonances to a Ca^{2+} titration in the HSQC spectrum (500 MHz) of PCaM. Amides are shown as spheres on the backbone structure of Ca^{2+}-saturated PCaM (1clm.pdb) (*62*). Red spheres indicate amides in slow exchange and blue spheres indicate amides in fast or intermediate exchange between the apo and Ca^{2+}-saturated states. Purple spheres indicate amides that demonstrate slow and fast exchange at different Ca^{2+} levels. Green spheres indicate no chemical shift change. Due to spectral overlap, the changes of many amide resonances could not be evaluated. Gold spheres indicate Ca^{2+} ions. This figure was generated using Molscript (*69*) and Raster3D software (*70*).

for turns in CaM (see Figure 20.B in ref *21*), and NMR studies showed them to be more dynamic in solution (*8*). This may allow the protein to adjust the tertiary arrangement of paired EF-hands to be energetically more favorable. The significance of residues in these regions has been underscored by studies of a mutant of calbindin D_{9k} (*58*) and mutants of PCaM (*55*).

Calcium Occupancy of Sites. Because most residues of the C-domain (85−148) were in slow exchange with respect to Ca^{2+} ligation (red spheres in Figure 8), changes in peak intensity were monitored. Excellent agreement was observed between the Cd^{2+} and Ca^{2+} titrations monitored by either the loss of intensity of a cross-peak of the apo state and/or the concomitant increase of intensity of the corresponding cross-peak of the Ca^{2+}-loaded state. The data show that the addition of the first 2 equiv of ion was required to complete the spectral transition.

Many of the residues monitored in the N-domain had intermediate exchange behavior (blue spheres in Figure 8) so changes in both their chemical shift and peak intensities were monitored. Line broadening of N-domain resonances (e.g., T26, I27, and T29) caused a decrease of peak intensities at low levels of Ca^{2+} (see Figure 4). This type of behavior is indicative of partial occupancy of the N-domain sites at these levels of Ca^{2+} (*57*, *59*) and has been observed in a calcium titration of cardiac troponin C (cTnC) (*60*), a closely related EF-hand protein. The change in amide resonance chemical shift was observed at higher Ca^{2+} levels as was expected for these lower affinity sites. Although the absolute change in amide resonance chemical shift varied from residue to residue, the normalized fractional change for each residue had a similar Ca^{2+} dependence. Therefore, it was apparent that sites I and II bound Ca^{2+} simultaneously.

Although Ca^{2+}-induced switching behavior in PCaM is approximately sequential by domain, Figure 5 demonstrates partial occupancy of sites I and II accompanies saturation of sites III and IV. Calcium binding is concerted within domains (sites III and IV filled simultaneously, as do sites I and II). These results are similar to those reported for *Drosophila* calmodulin, where the four residues in the eighth position of the 12-residue binding sites were used to monitor Ca^{2+} ligation (*57*), and with equilibrium Ca^{2+}-binding studies of PCaM and CaM (*33*).

PCaM is 88% identical in sequence to vertebrate CaM (see Figure 1B), with the majority of variations observed in the C-domain. There are two sequence differences in the interdomain linker region (Asp to Glu at position 78 and Thr to Gln at position 79; Figure 1B). Comparison of a crystal structure of vertebrate CaM [3cln.pdb (*61*)] to PCaM [1osa.pdb (*62*)] shows only a 0.53 Å RMS deviation in their α-carbon atoms. Comparison of Ca^{2+} binding to sites III and IV in PCaM and RCaM (*33*) indicates that these sites in PCaM have a higher affinity than the sites in RCaM. Comparative studies of isolated N-domain fragments (1−80) from PCaM and RCaM monitored using phenylalanine fluorescence (*55*) indicated that the six sequence differences in the PCaM fragment (two of which are in the interdomain linker) caused a decrease in Ca^{2+} affinity and increased the thermostability of the PCaM fragment (*28*).

Apparently these sequence differences widen the separation between the Ca^{2+} affinities of the two domains in PCaM relative to those of RCaM. This may provide a more complete separation of Ca^{2+}-dependent, domain-specific switching of PCaM. Such a postulate would be consistent with behavior of domain-specific functional mutants of *Paramecium* (*63*, *64*) and the failure of vertebrate CaM to restore function to *Paramecium* cells that are expressing a mutant form of PCaM known to be defective in regulating ion channels (*65*).

Conformational Changes in the Interdomain Linker Region. The role of the interdomain linker region in regulating the functional energetics of the N- and C-terminal domains is being actively investigated. The effect of adding residues 76−80 to N-domain fragments consisting of residues 1−75 of RCaM and PCaM was to decrease the Ca^{2+} affinity of sites I and II by a factor of 4 and increase the stability of the apo fragment by approximately 10 °C (*28*). Therefore, although these linker residues do not contact the calcium-binding sites per se, they have a significant effect on long-range regulation of the energetic properties of this domain. Detailed structural analyses of the Ca^{2+}-dependent properties of the interdomain linker are essential for understanding the relationship between the conformations of this region and function of calmodulin.

NMR solution studies of CaM in the absence (*6*, *7*) and presence of saturating Ca^{2+} (*8*, *25*−*27*) indicate that the interdomain region is dynamically disordered. These residues in the apo structure adopt a helical conformation one-third of the time (*6*), indicating that, in the absence of Ca^{2+}, the interdomain linker is considerably less flexible. Spectroscopic studies by Squier and co-workers have explored the mechanisms by which a Ca^{2+}-dependent change in this linker region can provide a structural coupling between the two domains that serves as a switch to regulate target activation (*29*−*32*). Their studies suggest that hydrogen bonding between E82 and Y138 may initiate the structural collapse of CaM observed upon target binding (*31*).

Recent analysis of NMR relaxation (*26*, *27*) and residual dipolar couplings (*25*) reveals a larger degree of flexibility in the interdomain linker and hydrophobic pockets of CaM than was previously thought. On the basis of crystallographic studies of PCaM, Wilson and Brunger have postulated that "the different activities of CaM in response to Ca^{2+} may result primarily from Ca^{2+}-mediated alterations in the dynamics of the protein" (*66*). Using $^{1}H-^{15}N$ HSQC NMR to monitor the Ca^{2+}-dependent conformational changes in the backbone atoms of PCaM, we demonstrate here that linker residues (E78 to E84) exhibit a domain-specific, Ca^{2+}-dependent response to binding in all four sites. More importantly, the chemical exchange behavior of these residues mimicked the exchange behavior of residues in the domain undergoing the greatest change in occupancy (slow exchange upon ligation of sites III and IV and fast exchange upon ligation of sites I and II). These studies support the proposal that the interdomain linker serves as a conformational switch that couples the Ca^{2+}-dependent properties of the two domains in CaM and is activated upon ligation of sites III and IV in the C-domain.

Structural vs Energetic Interactions. The issue of calcium-induced interdomain communication in CaM is widely debated. There are no persistent short-range contacts and the domains tumble freely, without a fixed orientation. A growing body of work demonstrates energetic coupling between the domains (*2*, *13*, *19*, *22*−*24*, *29*−*32*, *67*).

We focused on the contribution of the linker to this process because the thermostability and calcium-binding properties of N-domain fragments from two species of CaM demonstrated that residues in the linker region contribute to increasing thermostability while decreasing calcium affinity of sites I and II (*2*, *28*, *68*). Thus, it was clear that the difference in calcium-binding behavior of the domains within full-length CaM is not "intrinsic" to the sequences of the 12-residue EF-hand sites in each domain but depends on covalent connection of the two domains. Recent studies of calcium binding to cTnC revealed a similar phenomenon: calcium has a higher affinity for an N-domain fragment of cTnC than it does for the same site in full-length cTnC (*60*). We favor a model in which changes in tertiary contacts and dynamic properties induced by occupancy of sites III and IV exert an effect on the Ca^{2+}-binding properties of sites I and II via the linker region. However, the underlying mechanism for these distributed energetic effects is not yet understood and will require further studies with more sophisticated methods of dissecting residue-specific responses throughout CaM.

ACKNOWLEDGMENT

We thank Robert Cohen for the gift of ^{113}CdO, William Kearney and the University of Iowa College of Medicine NMR Facility for implementing the sensitivity-enhanced HSQC pulse sequence used in the Ca^{2+} titration, and John Snyder and the University of Iowa High-Field NMR Facility for the ^{113}Cd NMR parameters. We also thank Shapoor Riahi of the University of Iowa Department of Pediatrics for atomic absorption analyses, the University of Iowa Molecular Analysis Facility for amino acid analyses, and Andrew D. Robertson and Ian Armitage for helpful discussions.

SUPPORTING INFORMATION AVAILABLE

Changes in the chemical shift of particular atoms, a diagram of changes in residue-specific secondary structure in response to Ca^{2+} saturation, chemical frequency changes of amide protons in the N-domain, and complete NMR resonance assignments of backbone atoms of PCaM under apo and Ca^{2+}-saturating conditions. This material is available free of charge via the Internet at http://pubs.acs.org.

REFERENCES

1. Strynadka, N. C. J., and James, M. N. G. (1989) *Annu. Rev. Biochem. 58*, 951−998.
2. Sorensen, B. R., and Shea, M. A. (1998) *Biochemistry 37*, 4244−4253.
3. Linse, S., Helmersson, A., and Forsén, S. (1991) *J. Biol. Chem. 266*, 8050−8054.
4. Crouch, T. H., and Klee, C. B. (1980) *Biochemistry 19*, 3692−3698.
5. Wang, C.-L. A. (1985) *Biochem. Biophys. Res. Commun. 130*, 426−430.
6. Kuboniwa, H., Tjandra, N., Grzesiek, S., Ren, H., Klee, C. B., and Bax, A. (1995) *Nat. Struct. Biol. 2*, 768−776.
7. Zhang, M., Tanaka, T., and Ikura, M. (1995) *Nat. Struct. Biol. 2*, 758−767.
8. Barbato, G., Ikura, M., Kay, L. E., Pastor, R. W., and Bax, A. (1992) *Biochemistry 31*, 5269−5278.
9. Klevit, R. E., Dalgarno, D. C., Levine, B. A., and Williams, R. J. P. (1984) *Eur. J. Biochem. 139*, 109−114.
10. Ikura, M., Hiraoki, T., Hikichi, K., Mikuni, T., Yazawa, M., and Koichi, Y. (1983) *Biochemistry 22*, 2568−2572.
11. Dalgarno, D. C., Klevit, R. E., Levine, B. A., Williams, R. J. P., Dobrowolski, Z., and Drabikowski, W. (1984) *Eur. J. Biochem. 138*, 281−289.
12. Ikura, M., Hiraoki, T., Hikichi, K., Minowa, O., Yamaguchi, H., Yazawa, M., and Yagi, K. (1984) *Biochemistry 23*, 3124−3128.
13. Lee, S. Y., and Klevit, R. E. (2000) *Biochemistry 39*, 4225−4230.
14. Giedroc, D. P., Puett, D., Sinha, S. K., and Brew, K. (1987) *Arch. Biochem. Biophys. 252*, 136−144.
15. Giedroc, D. P., Sinhas, S. K., Brew, K., and Puett, D. (1985) *J. Biol. Chem. 260*, 13406−13413.

16. Mackall, J., and Klee, C. B. (1991) *Biochemistry 30*, 7242−7247.
17. Kawasaki, H., Kurosu, Y., Kasai, H., Isobe, T., and Okuyama, T. (1986) *J. Biochem. (Tokyo) 99*, 1409−1416.
18. Walsh, M., Stevens, F. C., Kuznicki, J., and Drabikowski, W. (1977) *J. Biol. Chem. 252*, 7440−7443.
19. Shea, M. A., Verhoeven, A. S., and Pedigo, S. (1996) *Biochemistry 35*, 2943−2957.
20. Pedigo, S., and Shea, M. A. (1995) *Biochemistry 34*, 1179−1196.
21. Shea, M. A., Sorensen, B. R., Pedigo, S., and Verhoeven, A. (2000) *Methods Enzymol. 323*, 254−301.
22. Starovasnik, M. A., Su, D. R., Beckingham, K., and Klevit, R. E. (1992) *Protein Sci. 1*, 245−253.
23. Martin, S. R., Maune, J. F., Beckingham, K., and Bayley, P. M. (1992) *Eur. J. Biochem. 205*, 1107−1114.
24. Maune, J. F., Klee, C. B., and Beckingham, K. (1992) *J. Biol. Chem. 267*, 5286−5295.
25. Chou, J. J., Li, S., Klee, C. B., and Bax, A. (2001) *Nat. Struct. Biol. 8*, 990−997.
26. Lee, A. L., Kinnear, S. A., and Wand, J. A. (2000) *Nat. Struct. Biol. 7*, 72−77.
27. Evenas, J., Forsén, S., Malmendal, A., and Akke, M. (1999) *J. Mol. Biol. 289*, 603−617.
28. Sorensen, B. R., Faga, L. A., Hultman, R., and Shea, M. A. (2002) *Biochemistry 41*, 15−20.
29. Sun, H., Yin, D., and Squier, T. C. (1999) *Biochemistry 38*, 12266−12279.
30. Yin, D., Sun, H., Ferrington, D. A., and Squier, T. C. (2000) *Biochemistry 39*, 10255−10268.
31. Sun, H., Yin, D., Coffeen, L. A., Shea, M. A., and Squier, T. C. (2001) *Biochemistry 40*, 9605−9617.
32. Qin, Z., and Squier, T. C. (2001) *Biophys. J. 81*, 2908−2918.
33. Jaren, O. R., Harmon, S., Chen, A. F., and Shea, M. A. (2000) *Biochemistry 39*, 6881−6890.
34. Wishart, D. S., Bigam, C. G., Yao, J., Abildgaard, F., Dyson, H. J., Oldfield, E., Markley, J. L., and Sykes, B. D. (1995) *J. Biomol. NMR 6*, 135−140.
35. Zhang, O., Kay, L. E., Olivier, J. P., and Forman-Kay, J. D. (1994) *J. Biomol. NMR 4*, 845−858.
36. Vuister, G. W., and Bax, A. (1992) *J. Magn. Reson. 98*, 428−435.
37. Grzesiek, S., and Bax, A. (1992) *J. Magn. Reson. 99*, 201−207.
38. Muhandiram, D. R., and Kay, L. E. (1994) *J. Magn. Reson., Ser. B 103*, 203−216.
39. Wittekind, M., and Mueller, L. (1993) *J. Magn. Reson., Ser. B 101*, 201−205.
40. Kay, L. E., Xu, G. Y., and Yamazaki, T. (1994) *J. Magn. Reson., Ser. A 109*, 129−133.
41. Clubb, R. T., Thanabal, V., and Wagner, G. (1992) *J. Magn. Reson. 97*, 213-217.
42. Swapna, G. V., and Montelione, G. T. (1999) *J. Magn. Reson. 137*, 437−442.
43. Marion, D., Ikura, M., Tschudin, R., and Bax, A. (1989) *J. Magn. Reson. 85*, 393−399.
44. Cavanagh, J., and Rance. M. (1990) *J. Magn. Reson. 88*, 72−85.
45. Kay, L. E., Keifer, P., and Saarinen, T. (1992) *J. Am. Chem. Soc. 114*, 10663−10665.
46. Palmer, A. G., Cavanagh, J., Byrd, R. A., and Rance, M. (1992) *J. Magn. Reson. 96*, 416−424.
47. Grzesiek, S., and Bax, A. (1993) *J. Biomol. NMR 3*, 185−204.
48. Lukin, J. A., Gove, A. P., Talukdar, S. N., and Ho, C. (1997) *J. Biomol. NMR 9*, 151−166.
49. Brokx, R. D., and Vogel, H. J. (2000) *Protein Sci. 9*, 964−975.
50. Andersson, A., Forsen, S., Thulin, E., and Vogel, H. J. (1983) *Biochemistry 22*, 2309−2313.
51. Gronenborn, A. M., and Clore, G. M. (1994) *J. Biomol. NMR 4*, 455−458.
52. Wishart, D. S., and Sykes, B. D. (1994) *Methods Enzymol. 239*, 363−392.
53. Klevit, R. E. (1983) *Methods Enzymol. 102*, 82−104.
54. Pedigo, S., and Shea, M. A. (1995) *Biochemistry 34*, 10676−10689.
55. VanScyoc, W. S., and Shea, M. A. (2001) *Protein Sci. 10*, 1758−1768.
56. Ikura, M., Minowa, O., and Hikichi, K. (1985) *Biochemistry 24*, 4264−4269.
57. Biekofsky, R. R., Martin, S. R., Browne, J. P., Bayley, P. M., and Feeney, J. (1998) *Biochemistry 37* , 7617−7629.
58. Nelson, M. R., Thulin, E., Fagan, P. A., Forsén, S., and Chazin, W. J. (2002) *Protein Sci. 11*, 198−205.
59. Sanders, J. K. M., and Hunter, B. K. (1990) in *Modern NMR Spectroscopy: A Guide for Chemists*, Oxford University Press, New York.
60. Li, M. X., Saude, E. J., Wang, X., Pearlstone, J. R., Smillie, L. B., and Sykes, B. D. (2002) *Eur. Biophys. J. 31*, 245−256.
61. Babu, Y. S., Bugg, C. E., and Cook, W. J. (1988) *J. Mol. Biol. 204*, 191−204.
62. Rao, S. T., Wu, S., Satyshur, K. A., Ling, K.-Y., Kung, C., and Sundaralingam, M. (1993) *Protein Sci. 2*, 436−447.
63. Kung, C., Preston, R. R., Maley, M. E., Ling, K.-Y., Kanabrocki, J. A., Seavey, B. R., and Saimi, Y. (1992) *Cell Calcium 13*, 413−425.
64. Ling, K.-Y., Preston, R. R., Burns, R., Kink, J. A., Saimi, Y., and Kung, C. (1992) *Proteins: Struct., Funct., Genet. 12*, 365−371.
65. Hinrichsen, R. D., Burgess-Cassler, A., Soltvedt, B. C., Hennessey, T., and Kung, C. (1986) *Science 232*, 503−506.
66. Wilson, M. A., and Brunger, A. T. (2000) *J. Mol. Biol. 301*, 1237−1256.
67. Small, E. W., and Anderson, S. R. (1988) *Biochemistry 27*, 419−428.
68. Faga, L. A., Sorensen, B. R., VanScyoc, W. S., and Shea, M. A. (2002) *Proteins: Struct., Funct., Genet.* (in press).
69. Kraulis, P. J. (1991) *J. Appl. Crystallogr. 24*, 946−950.
70. Merritt, E. A., and Bacon, D. J. (1997) *Methods Enzymol 277*, 505−524.

BI026340+